Available online at www.sciencedirect.com

SciVerse ScienceDirect

Ceramics International 39 (2013) 3007–3015

CERAMICS INTERNATIONAL

www.elsevier.com/locate/ceramint

Effect of fuel to oxidant molar ratio on the photocatalytic activity of ZnO nanopowders

M. Ahmad[a,b,*], Zhanglian Hong[a,**], E. Ahmed[b], N.R. Khalid[a,b], A. Elhissi[c], W. Ahmad[c]

[a]State Key Laboratory of Silicon Materials and Department of Materials Science and Engineering, Zhejiang University, Hangzhou 310027, PR China
[b]Department of Physics, Bahauddin Zakariya University, Multan 60800, Pakistan
[c]Institute of Nanotechnology and Bioengineering, University of Central Lancashire Preston PR1 2HE, UK

Received 28 June 2012; received in revised form 12 September 2012; accepted 21 September 2012
Available online 3 October 2012

Abstract

In this study, the effects of fuel to oxidant (F/O) molar ratio on the characteristics and photocatalytic activity of ZnO nano-powders were investigated. A simple and inexpensive combustion process was utilized to synthesize the nano-powders. A range of analytical techniques including X-ray diffraction (XRD), Scanning electron microscopy (SEM), Transmission electron microscopy (TEM), Fourier transform infrared spectroscopy (FTIR), UV–vis diffuse reflectance spectroscopy (DRS) and Photoluminescence spectroscopy (PL) were employed to characterize the nano-powders. XRD patterns showed that the synthesized powders have hexagonal wurtzite structure and high crystallinity without any secondary phase. The calculated crystallite size was in the range of 35–29 nm which decreased by increasing the F/O ratio. UV–vis diffuse reflectance spectroscopy showed a gradual shift of optical absorption spectra in the visible region of light when F/O ratio was increased. PL spectroscopy confirmed that the prepared photocatalysts had better charge separation capability as compared to the commercial ZnO. The photocatalytic activity of different samples was investigated by degradation of methyl orange (MO) dye under UV and visible light irradiation. The results demonstrated that F/O ratio had a significant influence on photocatalytic degradation of methyl orange compared to the commercially available ZnO and TiO_2 powders. Moreover, the photocatalysis of ZnO (F/O = 1.7) powder with particle size (31 nm) showed excellent performance for photodegradation of MO, which suggests a balance among the recombination rate, surface hydroxyl groups and specific surface area.
© 2012 Elsevier Ltd and Techna Group S.r.l.. All rights reserved.

Keywords: Powders; ZnO; Optical properties; Photocatlysis

1. Introduction

Industrial wastewater contains various organic and inorganic pollutants, which are generally toxic and resistant to destruction by biological methods of treatment. The conventional methods previously used for wastewater detoxification includes coagulation, flocculation, filtration, carbon adsorption process and treatment with ozone [1,2]. Unfortunately, these biological methods are ineffective due to high concentration and stability of organic dyes in the wastewater [3]. The photocatalytic process using nanostructured semiconductors is one of the technologies used for the destructive oxidation of organic compounds such as dyes [4]. Among these semiconductors, TiO_2 and ZnO have extensively been studied in the field of photocatalysis [5]. However ZnO has higher photocatalytic efficiency than TiO_2 due to its strong absorption of UV light from the solar spectrum [6,7]. Moreover, ZnO is an efficient photocatalyst for waste-water detoxification because it produces H_2O_2 more efficiently than any other photocatalysts [8].

Surface defects and interface properties of metal oxide nanoparticles also play an important role in photocatalysis. Nanoparticles with high specific surface area can provide surface states within the semiconductor band gap to enhance the photocatalytic activity especially in the visible light region. It has been previously found that photocatalysis efficiency can

*Corresponding author at: Department of Physics, Bahauddin Zakariya University, Multan 60800, Pakistan. Tel.: +92 61 9210091; fax: +92 61 9210098.
**Corresponding author. Tel./fax: +86 571 87951234.
E-mail addresses: mzkhm73@gmail.com (M. Ahmad), hong_zhanglian@zju.edu.cn (Z. Hong).

0272-8842/$ - see front matter © 2012 Elsevier Ltd and Techna Group S.r.l.. All rights reserved.
http://dx.doi.org/10.1016/j.ceramint.2012.09.079

be enhanced via optimizing of particle size of the ZnO photocatalyst [9,10]. However, preparation method and calcination temperature both strongly affect the properties of ZnO photocatalyst. Many techniques have been developed to synthesize nanocrystalline ZnO powders, including the co-precipitation method, sol–gel, intensive mechanical milling, spray pyrolysis, solution coating and combustion synthesis etc. [11–17]. Among these, the combustion synthesis appears to be the first choice for large scale economical production of nanopowders [18]. Sousa et al. have investigated the synthesis of pure and doped ZnO nanopowders by the combustion method using urea as a fuel and a good control over the compositions was observed [16]. Hwang and Wu have used the combustion method with glycine as a fuel to prepare ZnO nanopowders for their potential applications in electronic devices such as varistor [17].

In this study, the effects of the fuel to oxidant molar ratios on the properties of nanocrystalline ZnO photocatalysts were investigated using a single step chemical combustion process of preparation. The photocatalytic activity of the synthesized samples was studied by observing the degradation of the MO dye under ultraviolet (UV) and visible light irradiation. Also the effects of particle size on the optical properties and photocatalytic activity of nanocrystalline ZnO photocatalysts were evaluated.

2. Experimental

2.1. Catalysts preparation

Nanocrystalline ZnO photocatalysts were synthesized using a simple and inexpensive combustion method [17]. Zinc nitrate (oxidant) and glycine (fuel) were used for the preparation of ZnO nanopowders as elucidated in Fig. 1. The reagents were directly mixed at room temperature in the desired molar ratio. The nature of the fuel and its amount are important in combustion process for acquiring the transparent viscous gel without any phase separation or precipitation. Since zinc nitrate is hygroscopic, the mixture easily absorbs moisture from the surrounding environment, resulting in conversion of the material into transparent slurry. This slurry was dehydrated to form a gel by using a hot plate (90–100 °C). Precursor/gel was further ignited by heating on the hot plate at ~180–200 °C. During the combustion reaction, large amounts of heat and non-toxic gases were explosively generated, resulting in formation of dry and voluminous nanocrystalline ZnO powders. It was noted that the color of synthesized powders was changed from off-white to yellow, yellow to light brown, light brown to brown and finally brown to black for F/O=1.1, 1.4, 1.7, 2.1and 2.5 respectively. Finally, the prepared samples were calcined at 500 °C for 3 h in the furnace.

2.2. Catalyst characterization

Powder X-ray diffraction (XRD) patterns for samples were investigated using a Rigaku Dmax-IIIA X-ray diffractometer with Ni-filtered Cu-Kα radiation source at 40 kV and 36 mA. From the X-ray diffractograms, the average crystallite size was calculated using Scherer's formula. The surface morphology, particle size and compositional analysis of photocatalysts were studied using a scanning electron microscope (SEM), Hitachi S-4800 combined with EDX, transmission electron microscope (TEM), JEOL JEM 1200EX and high resolution transmission electron microscope (HRTEM) FEI TECNAI G^2 F20. The samples for SEM and TEM were prepared by dispersing the powders in ethanol via sonication and then dispersion was dropped on silicon coated glass slide and carbon coated copper grid respectively. UV–vis diffuse reflectance spectra (DRS) were measured in the range of 300–800 nm using a Hitachi U-4100 UV–vis-spectrometer equipped with an integrating sphere of 60 mm using $BaSO_4$ as a standard. The PL emission spectra were recorded using a Hitachi F-4500 fluorescence spectrophotometer. The samples excitation was performed at 325 nm at room temperature and the emission was scanned between 350 and 630 nm. Fourier transform infrared (FT-IR) spectra were recorded at room temperature in 4000–400 cm^{-1} range using Nicolet Avatar 360 FT-IR with KBr pellet method.

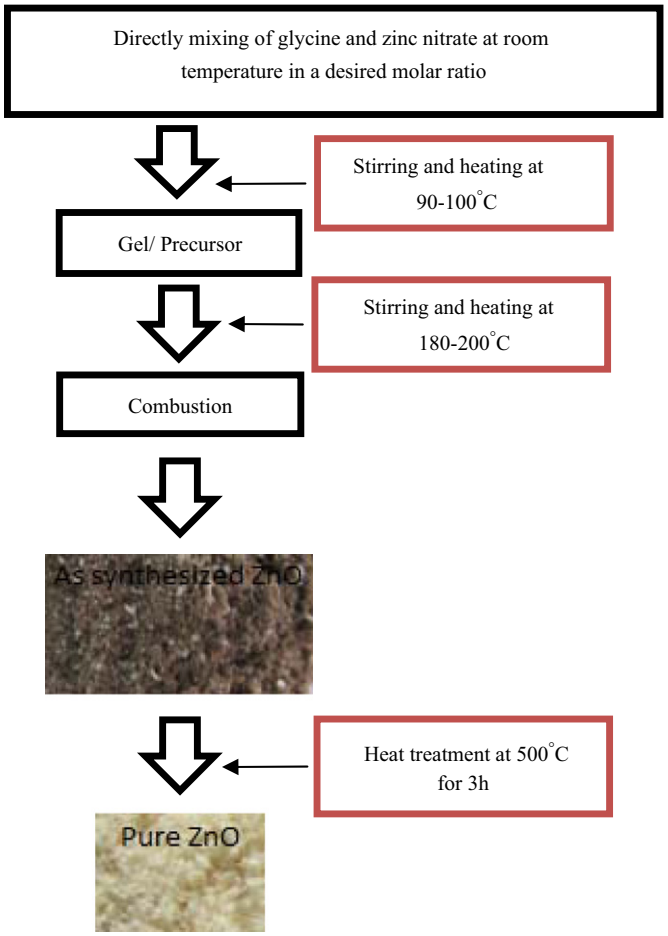

Fig. 1. Flow chart for the synthesis of ZnO nanopowders.

2.3. Measurement of photocatalytic activity

The photocatalytic activity of ZnO powders were estimated by monitoring the degradation of MO (Fig. 2a) as a model compound in a self-assembled apparatus with a metal halogen lamp (HQIBT, 400 W/D, OSRAM, Germany) as the radiation source. In the present investigation, photocatalytic activities under visible as well as UV light were studied. The visible light ($\lambda \geq 420$ nm) used in the present study was obtained by using a filter with cut-off wavelength of 420 nm. The UV–visible spectrum of the dye in aqueous medium is shown in Fig. 2(b). The peak at 464 nm was used to monitor the photocatalytic degradation of MO. For the photocatalytic experiment, 50 mg photocatalysts were suspended in MO aqueous solution (50 mL) with a concentration of 10 mg/L in a beaker. The suspension was magnetically stirred for 30 min to reach the adsorption/desorption equilibration without light exposure. Following this, the photocatalytic reaction was started by the exposure of the desired light. The temperature of the suspension was kept at about 20 °C by an external cooling jacket with recycled water. After a setup exposure time, 3 mL suspension was sampled, centrifuged and the supernatant was taken out for UV–vis absorption spectrum measurement (Hitachi U-4100 UV–vis spectrometer). The intensity of the main absorption peak of the MO dye was referred to as the measure of the residual dye concentration.

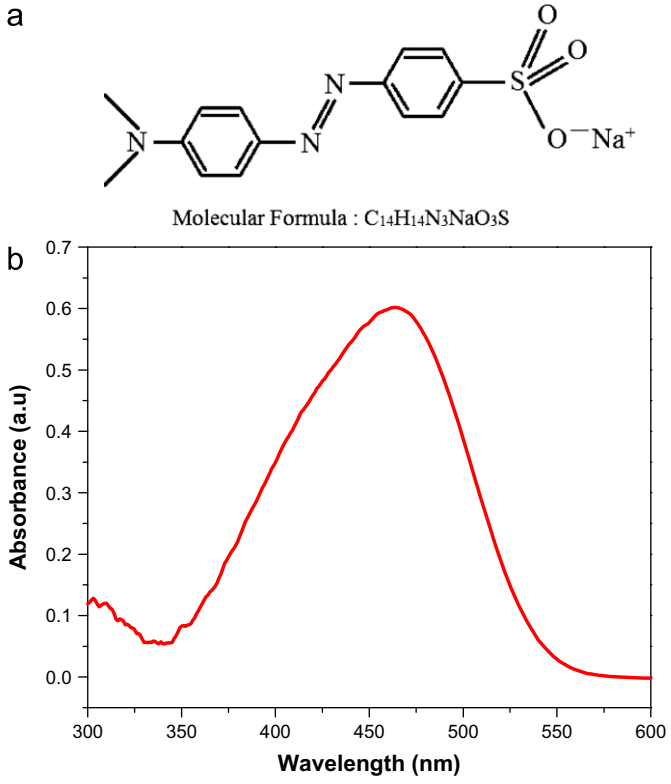

Fig. 2. (a) The structural and chemical formula of MO and (b) the UV–visible absorption spectrum of MO.

3. Results and discussion

Fig. 3 shows the XRD patterns of ZnO samples. All of the nanocrystalline ZnO powders synthesized for the range of fuel to oxidant molar ratio (F/O = 1.1–2.5) revealed quite sharp X-ray diffraction peaks indicating crystallinity of the samples. These XRD patterns clearly showed 10 main peaks of hexagonal wurtzite structure of ZnO, namely, the planes (100), (002), (101), (102), (110), (103), (200), (112), (201) and (202), which all are in good agreement with JCPDS-05-0664 and literature findings [19–21]. The lattice constant corresponding to the main peak of ZnO at $2\theta = 36.3^\circ$ were obtained by the following equation:

$$I/d^2_{hkl} = 4/3\left(h^2 + hk + k^2\right)/a^2 + l^2/c^2$$

The average values of lattice constant calculated by using the above equation are "$a = 3.2538$ Å" and "$c = 5.2134$ Å". These calculated values of lattice constants are in good agreement with standard data ($a = 3.249$ Å and $c = 5.206$ Å) [19]. The crystallite size was estimated using the full width at half maximum (FWHM) of high intensity peak (101) appear at $2\theta = 36.3^\circ$ using Scherer's formula:

$$d = k\lambda/\beta \cos\theta$$

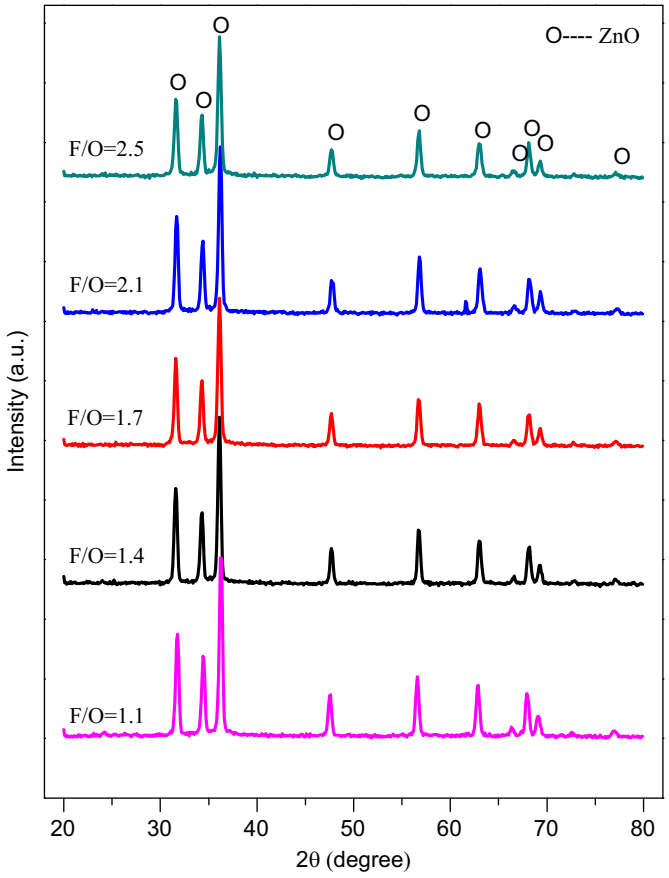

Fig. 3. X-Ray diffraction patterns of ZnO nanopowders with different F/O values.

where "d" is the crystallite size in nanometers, $k=0.89$ which is a constant, λ is the wavelength of X-ray radiation in nanometers, θ is the Bragg angle in radians and β is the FWHM in radians. The results show that the particles obtained by the combustion process were nanocrystalline with size in the range of 35–29 nm (Fig. 4).

Fig. 5(a,c,d) showed that the morphology of representative sample ZnO (F/O=1.7) nanoparticles, examined under SEM, TEM and HRTEM respectively. The images of ZnO demonstrated clusters of very small and highly uniform nanocrystalline grains with a loose appearance. This porous morphology observed is caused by the liberation of large amount of gases during the combustion reaction. It is also noted that lattice fringes of ZnO nanoparticles were sharper, indicating high crystallinity of the nanoparticles. The observed particle sizes and crystallinity are in good agreement with XRD results. The chemical composition of ZnO (F/O=1.7) powders was examined by EDX measurements and is shown in Fig. 5(b). The EDX analysis showed the weight and atomic percentages of zinc and oxygen (Zn/O) in the sample and values are presented in Table 2.

Fig. 6(a) shows the diffuse reflectance spectra of ZnO samples measured in the 300–600 nm wavelength range. The absorption spectra from reflectance data were obtained by application of the Kubelka–Munk algorithm and are shown in Fig. 6(b). The absorption spectra of ZnO powders synthesized with different fuel to oxidant molar

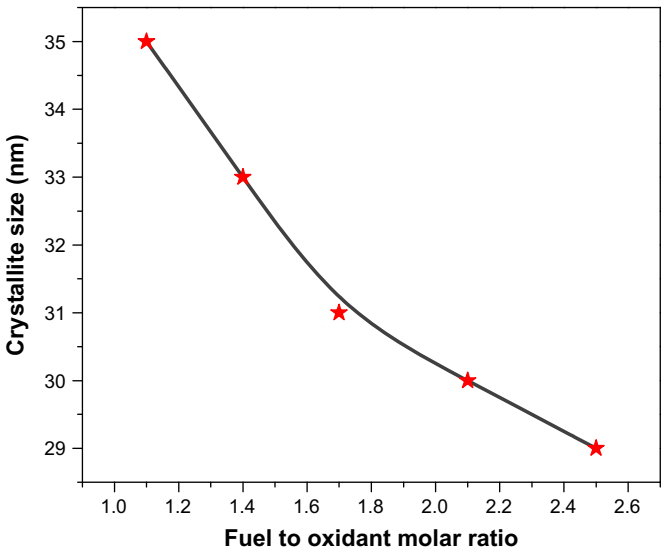

Fig. 4. Plot of crystallite size as a function of F/O molar ratio.

Table 1
Detail of crystallite size and band gap for different F/O values.

F/O molar ratio	Crystallite size	Band gap
1.1	35	3.263
1.4	33	3.260
1.7	31	3.257
2.1	30	3.251
2.5	29	3.248

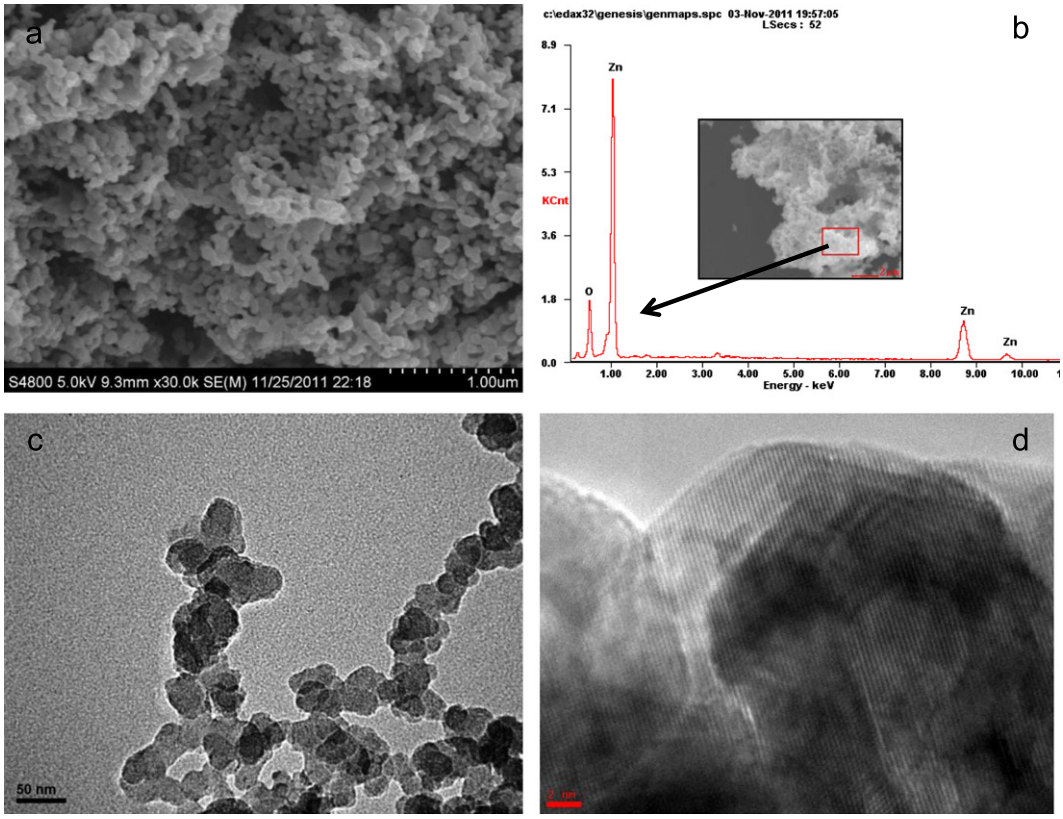

Fig. 5. (a) SEM image, (b) EDX spectra, (c) TEM image and (d) HRTEM image of the ZnO (F/O=1.7).

ratios shifted to visible light region. This type of modification in optical properties can be attributed to charge transfer from O^{2-} to Zn^{2+} responsible for the band-gap [22]. Band gap energy can be estimated from the absorption spectra. Semiconductors are classified to be direct or indirect according to the lowest allowed electronic transition. Direct band semiconductors are characterized by the minimum of the lowest conduction band position in k-space directly under the maximum of the highest valance band. The relation between absorption coefficient (α) and incident photon energy ($h\upsilon$) for allowed direct transitions can be presented as

$$(\alpha h\upsilon)^2 = A\left(h\upsilon - E_g\right)$$

Table 2
Weight and atomic percentage of zinc and oxygen (Zn/O) in ZnO (F/O=1.7).

Element	Weight%	Atomic%
O	20.31	50.53
Zn	79.69	49.47
Total	100	100

where A is the absorption constant. The plots of $(\alpha h\upsilon)^2$ versus $h\upsilon$ from the spectral data of Fig. 6(b) are presented in Fig. 6(c). By extrapolating the linear portion of the curve to zero absorbance, the direct band gap energy values of the ZnO powders can be estimated. Table 1 shows the band gap energy values of different photocatalysts. The band gap energy values decrease due to the decrease in particle size of ZnO powders. [23–25]. It can also be seen that the slope of UV–vis absorption spectra of ZnO powders was steeper for the sample having smaller particle size of 29 nm. A sharp UV–vis absorption curve (steep slope) indicates a high degree of crystallinity [23].

The photoluminescence emission spectra is advantageous for investigation of the effectiveness of charge carrier trapping, imigration, transfer and in understanding the fate of electron–hole pairs in semiconductor nanoparticles [26]. To study the effect of fuel to oxidant molar ratio on the photoluminescence of ZnO powders, the room temperature photoluminescence measurements were carried out at the excitation wavelength of 325 nm. The PL spectra of different ZnO photocatalysts are shown in Fig. 6(d). A strong UV emission at 385 nm and several relatively weak visible emissions in the range of 400–590 nm were

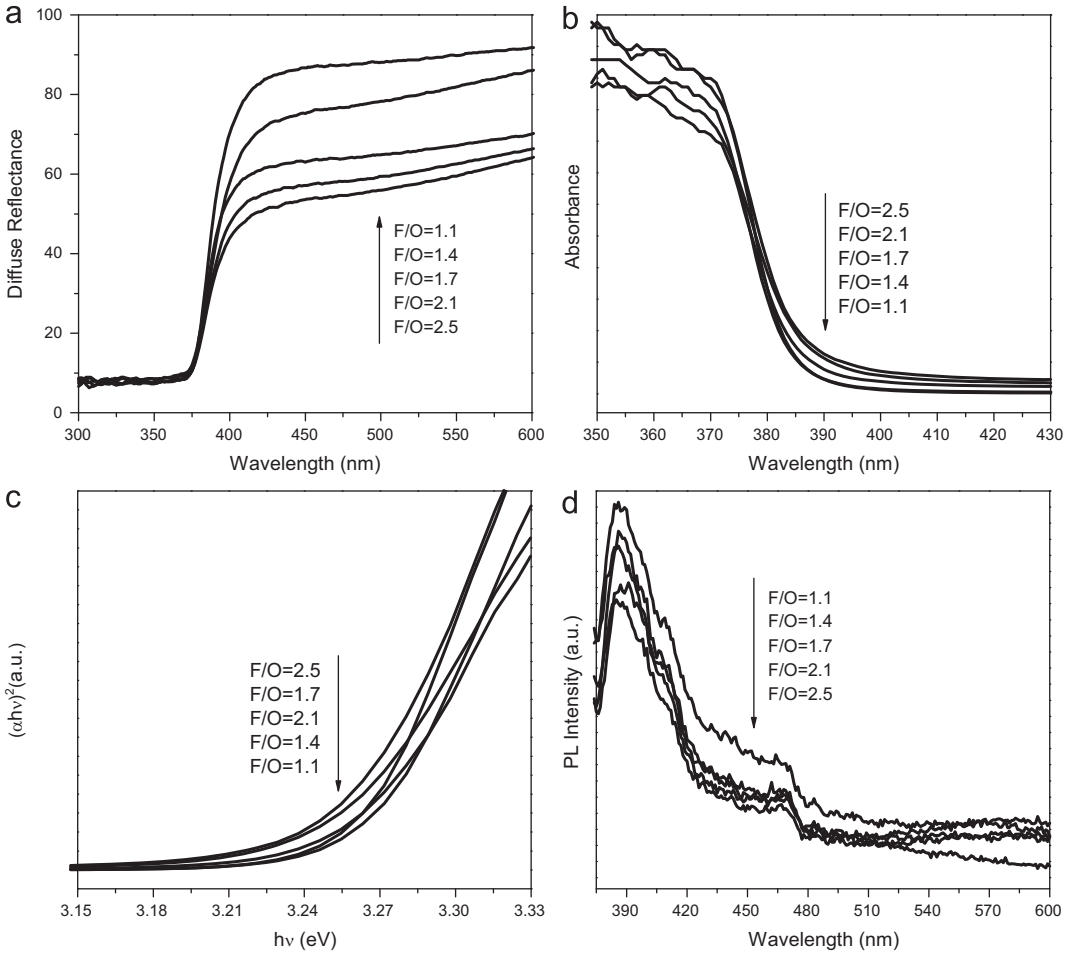

Fig. 6. Diffuse reflectance spectra (a) UV–vis absorption spectra (b) the $(\alpha h\upsilon)^2$ versus $h\upsilon$ curves for band gap determination (c) and photoluminescence spectra (d) of ZnO powders with different F/O values.

observed. The UV emission is attributed to free excitonic emission near the band edge and the visible emissions may be due to the transition from various kinds of defect states [27,28]. It was observed that the positions of the peaks were almost similar, while PL intensities were quite different among these samples. It is known that the PL emission is caused by the recombination of excited electrons and holes, and the lower PL intensity may indicate the lower recombination rate of electrons and holes under light irradiation. The PL intensity of ZnO (F/O = 1.1) is highest among all the samples, indicating the highest recombination of electrons and holes. The emission intensities were significantly weakened with the increase in F/O ratio, implying that the recombination of charge carriers was effectively suppressed. Among all the samples the lowest intensity was observed for ZnO (F/O = 2.5). This indicates that the charge carriers were separated more effectively.

The FT-IR spectra for the ZnO powders were obtained at the room temperature as shown in Fig. 7. A few distinct bands were observed in the high wave number region, at ~3440, ~2920, ~2850, ~1640, and ~1385 cm^{-1}. The peaks at 3440 and 1640 cm^{-1} imply that the basic hydroxyl groups of chemisorbed and/or physisorbed H_2O molecules

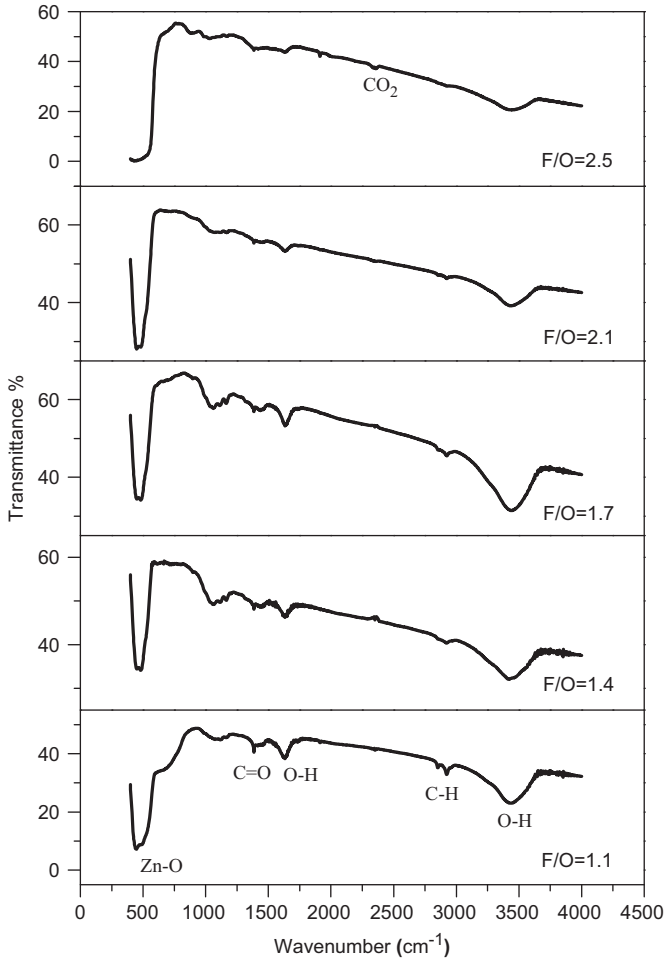

Fig. 7. FT-IR spectra of ZnO powders with different F/O values.

are present in all ZnO powders with the hydroxylated surfaces [29]. The bands at ~2920 and ~2850 cm^{-1} correspond to C–H stretching [30]. Another IR peak at ~1385 cm^{-1} results from OH^- absorption of hydrogen-related defects [29]. As the F/O ratio increases, the intensity of all IR peaks except the one at ~440 cm^{-1} becomes weaker step by step [21]. In addition, a strong absorption band corresponding to the stretching and vibrational modes of metal–oxygen bands (Zn–O) was also observed for each powder sample at ~440 cm^{-1} [21,31]. The shape of the IR spectrum of ZnO particles is generally influenced by particle size, morphology, the degree of particles aggregation and the crystal structure of the ZnO polymorph [32].

The photocatlytic activities of ZnO powders were studied by photodegradation of MO as model dye under UV as well as visible light. A blank experiment study of MO degradation without catalyst under the same condition was also observed. The results indicate that the mere photolysis can be ignored as the corresponding degradation is about 0.3% after illumination for 2 h. The photocatalytic performances for MO degradation by the ZnO catalysts are shown as plots of C/C_0(%) versus t (min) in Fig. 8. About 8% of the MO was adsorbed for ZnO (having F/O of 1.7) upon stirring for 30 min in the dark and it increased to some extent in comparison to other ZnO powders. Photocatalytic degradation of MO follows roughly the pseudo-first-order reaction kinetics for low dye concentrations

$$\ln(C_0/C) = k_{app}t$$

where k_{app} is the apparent constant, used as the basic kinetic parameter for different photocatalysts. C_0 is the initial concentration of MO in aqueous solution and C is the residual concentration of MO at time t. The apparent constant values could be deduced from the linear fitting of $\ln(C_0/C)$ versus irradiation time. The initial degradation rate ($r_0 = k_{app}C_0$) of 10 mgL^{-1} MO with different catalysts was studied and the results are presented in Fig. 9. The degradation rate of MO is in the order; ZnO (F/O = 1.7) > ZnO (F/O = 2.1) > ZnO (F/O = 2.5) > ZnO (F/O = 1.4) > ZnO (F/O = 1.1). The degradation rate under UV and visible light for ZnO (F/O = 1.7) catalyst was found superior to commercially available P-25 and ZnO (Fig. 9).

The dependence of percentage conversion of MO decomposition on the particle size of ZnO powders after time 't' is shown in Fig. 10. The percentages of MO degradation after 1 h increased from 78% to 100% under UV and from 2% to 25% under visible light when the particle size of ZnO powders decreased from 35 to 31 nm. For the smaller particle sizes (30–29 nm) of ZnO powders, the percentages of MO degradation gradually decreased from 100% to 97% under UV and from 25% to 11% under visible light. Therefore, 31 nm (for ZnO F/O = 1.7) is an optimum particle size of ZnO for maximum photocatalytic activity of the catalyst.

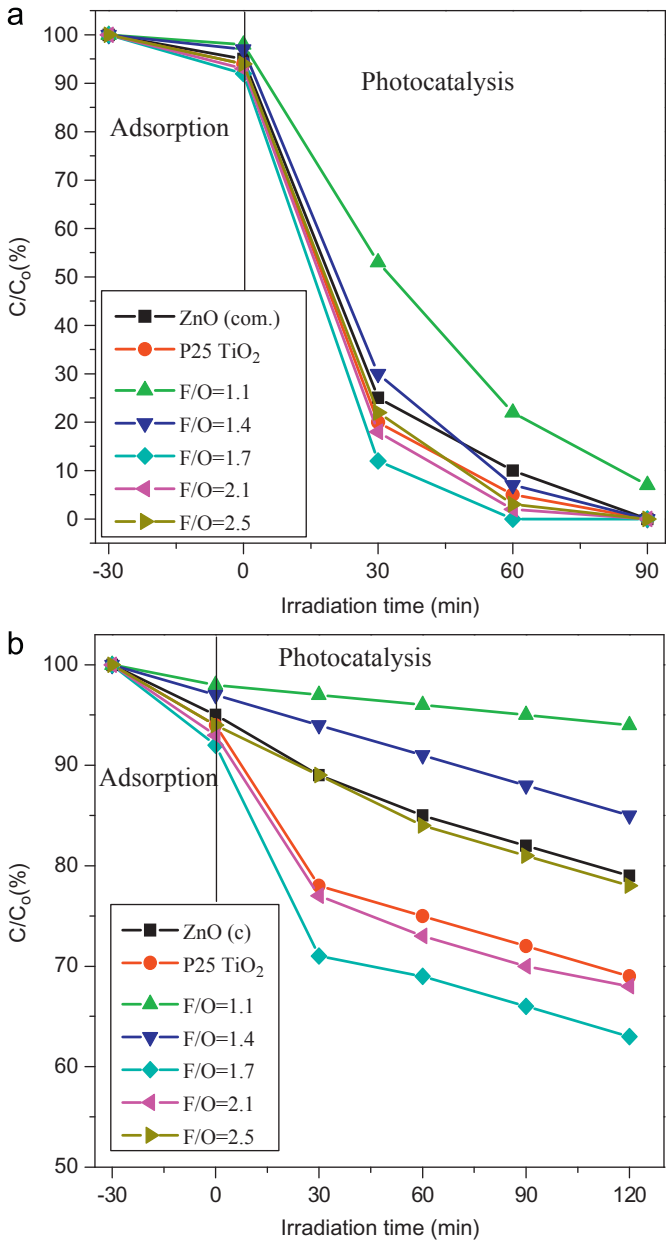

Fig. 8. Time profiles of C/C_o for various catalysts under (a) UV light and (b) visible light irradiation.

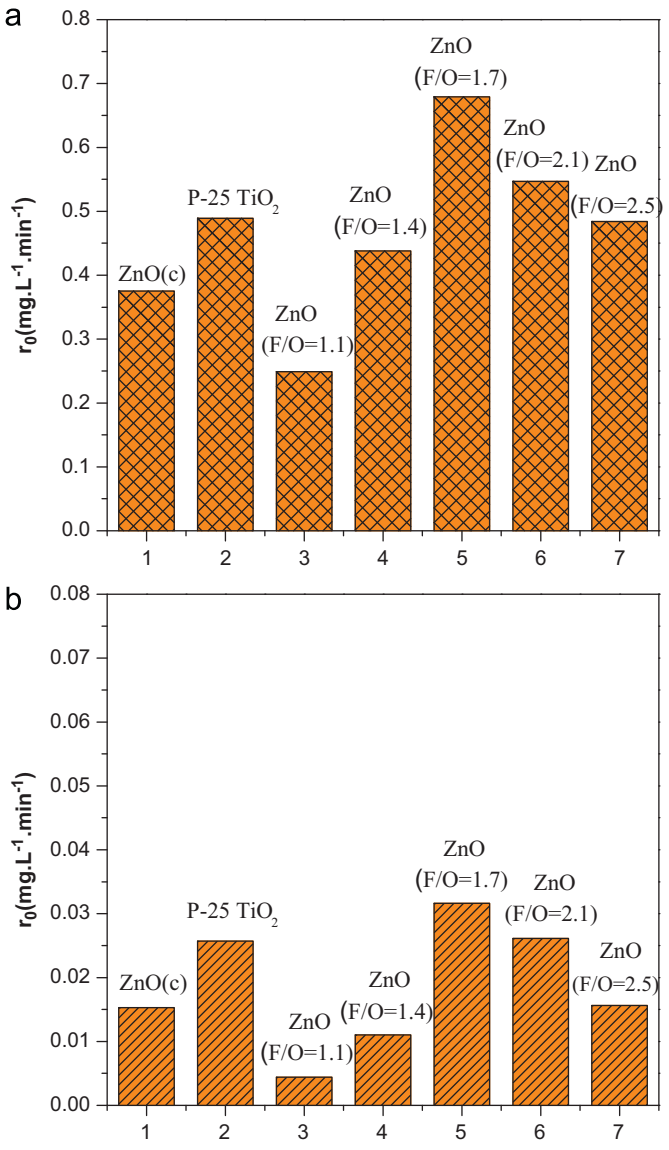

Fig. 9. The initial degradation rate of MO in the presence of various catalysts under (a) UV light and (b) visible light irradiation.

In general, photocatalysis can be considered to be dominated by the following linked mechanisms, namely recombination of electron-hole pair and surface catalytic effects [33]. Surface hydroxyl groups contribute in the photocatalytic process in a number of ways. They trap photoexcited electrons and create $OH^{\bullet}$ radicals. They can also act as active sites for the pollutants [34]. Recombination is a major limitation in semiconductor photocatalysis as it decreases the overall quantum efficiency of the photocatalyst due to high recombination rate of photo-induced electron–hole pair at the surface of the catalyst [35]. When recombination occurs, the excited electron returns to the valence band without reacting with adsorbed species [36]. Radiation may be emanated when an excited electron recombines with the hole in valence band. As such, photoluminescence (PL) can successfully be employed to monitor low intensity signals corresponding to lower recombination rates [35]. According to PL results, ZnO photocatalyst with lower F/O ratio should exhibit lower photocatalytic activity and must increase with increasing F/O ratio. However, it was noted that the photocatalytic activity initially increased with a maximum at F/O=1.7 and then decreased for higher molar ratios. On the other hand, surface hydroxyl groups were decreased with increasing F/O ratio; herein the photocatalyst with the lowest molar ratio (ZnO F/O=1.1) should show best photocatalytic activity [34]. The specific surface area also plays a vital role during photocatalysis, because large surface area will result in an increase in the number of active sites existing for degradation reactions. According to results, the photocatalyst with moderate molar ratio

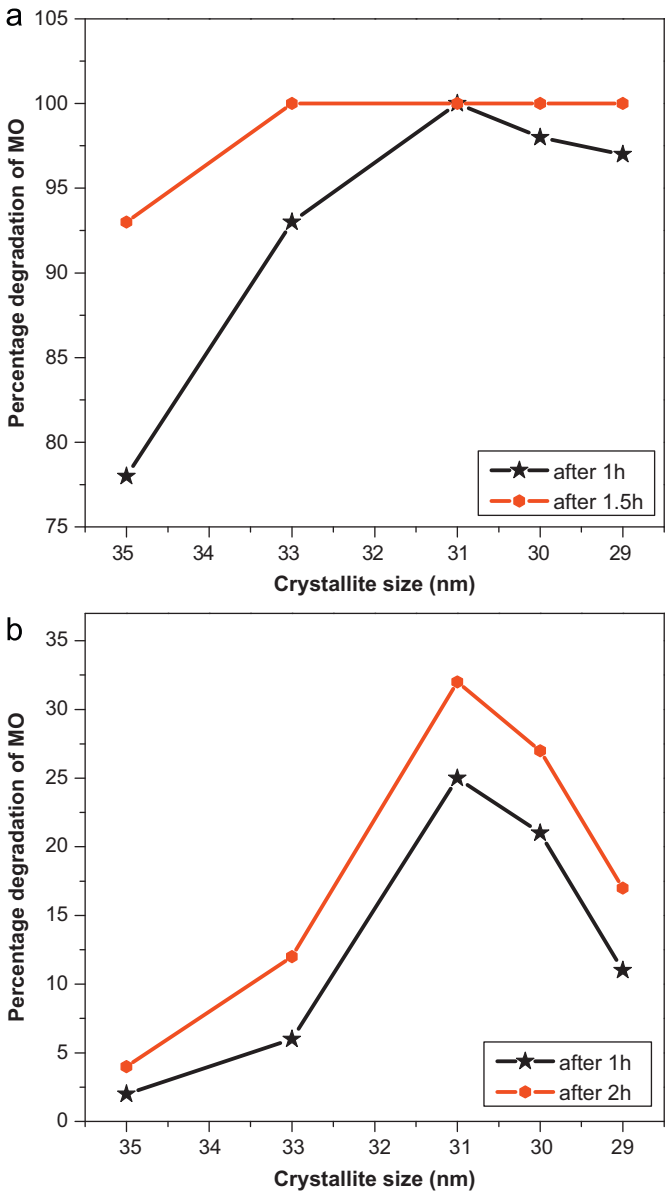

Fig. 10. Relationship between the percentage of MO degradation and the particle size of ZnO photocatalysts under (a) UV light and (b) visible light irradiation.

(ZnO F/O=1.7) exhibited best photocatalytic activity which may be attributed to the delicate balance among recombination rate, surface hydroxyl groups and specific surface area available for substrate adsorption.

4. Conclusions

ZnO nanopowders were successfully synthesized by the combustion technique and the effect of fuel to oxidant molar ratio on the photocatalytic activity was studied. The F/O molar ratio significantly affected the particle size, the optical and photocatalytic properties of ZnO powders. The absorption edge analysis showed that the band gap energy for the ZnO powders decreased with increasing F/O ratio. The ZnO (F/O=1.7) photocatalyst exhibited enhanced photo degradation of MO dye under UV and visible light irradiation.

Acknowledgments

This work was supported partially by the State Key Laboratory of Silicon Materials (SKL2009-14) at Zhejiang University. The authors also thank the Higher Education Commission of Pakistan for IRSIP scholarship.

References

[1] R.H. Souther, T.A. Alspaugh, Textile waste treatment studies, Journal of the Water Pollution Control Federation 29 (1957) 804.
[2] A. Hamza, M.F. Hamoda, Proceedings of the 35th Purdue Industrial Waste Congress, West Lafayette, IN, USA, 1980.
[3] J.P. Lorimer, T.J. Mason, M. Plattes, S.S. Phull, D.J. Walton, Degradation of dye effluent, Journal of Pure and Applied Chemistry 12 (2001) 1957–1968.
[4] N.S. Allen, M. Edge, J. Verran, J. Stratton, J. Maltby, C. Bygott, Photocatalytic titania based surfaces: environmental benefits, Polymer Degradation and Stability 9 (2008) 1632–1646.
[5] S. Sakthivel, B. Neppolian, M.V. Shankar, B. Arabindoo, M. Palanichamy, V. Murugesan, Solar photocatalytic degradation of azo dye comparison of photocatalytic efficiency of ZnO and TiO_2, Solar Energy Materials and Solar Cells 77 (2003) 65–82.
[6] K. Tanaka, K. Padermpole, T. Hisanaga, Photocatalytic degradation of commercial azo dyes, Water Research 34 (2000) 327–333.
[7] A. Sharma, P. Rao, R.P. Mathur, S.C. Ameta, Photocatalytic reactions of xylidine ponceau on semiconducting zinc oxide powder, Journal of Photochemistry and Photobiology A: Chemistry 86 (1995) 197–200.
[8] E.R. Carraway, A.J. Hoffman, M. Hoffmann, Photocatalytic oxidation of organic acids on quantum-sized semiconductor colloids, Environmental Science and Technology 28 (1994) 786–793.
[9] A.C. Dodd, A.J. McKinley, M. Saunders, T. Tsuzuki, Effect of particle size on the photoactivity of nanoparticulate zinc oxide, Journal of Nanoparticle Research 8 (2006) 43–51.
[10] D. Li, V. Balek, N. Ohashi, T. Mitsuhashi, S. Hishita, H. Haneda, Self-assembly prismatic aggregates formed during the calcination of ZnO powders: in situ monitoring by ETA technique and their photocatalytic properties, Journal of Colloid and Interface Science 289 (2005) 472–478.
[11] S.C. Pillai, J.M. Kelly, D.E. McCormack, P. O'Brien, R. Ramesh, The effect of processing conditions on varistors prepared from nanocrystalline ZnO, Journal of Materials Chemistry 13 (2003) 2586–2590.
[12] R.N. Viswanath, S. Ramasamy, R. Ramamoorthy, P. Jayavel, T. Nagarajan, Preparation and characterization of nanocrystalline ZnO based materials for varistor application, Nanostructured Materials 6 (1995) 993–996.
[13] R. Schulz, S. Boily, A. Joly, A.V. Neste, H. Alamdari, Varistor based on nanocrystalline powder produced by mechanical grinding, US Patent: US6 (2003) 620346B1.
[14] K. Hembram, R. Vijay, Y.S. Rao, T.N. Rao, Doped nanocrystalline powders for non-linear resistor application by spray pyrolysis method, Journal of Nanoscience and Nanotechnology 9 (2009) 4376–4382.
[15] S.A. Seyyed, M.M. Shahraki, M.A.F. Sani, A. Nemati, A. Yousefi, Microstructural and electrical properties of varistors prepared from coated ZnO nanopowders, Journal of Material Science: Materials in Electronic 21 (2010) 571–577.
[16] V.C. Sousa, A.M. Segadaes, M.R. Morelli, R.H.G.A. Kiminami, Combustion synthesized ZnO powders for varistor ceramics, International Journal of Inorganic Materials 1 (1999) 235–241.

[17] C.C. Hwang, T.Y. Wu, Synthesis and characterization of nanocrystalline ZnO powders by a novel combustion synthesis method, Materials Science and Engineering B 111 (2004) 197–206.
[18] K.C. Patil, S.T. Aruna, T. Mimani, Combustion synthesis: an update, Current Opinion in Solid State and Materials Science 6 (2002) 507–512.
[19] Joint Committee on Powder Diffraction Standards (JCPDS), File no. 05-0664.
[20] U. Ozgur, Y.I. Alivov, C. Liu, A. Teke, M.A. Reshchikov, S. Dogan, V. Avrutin, S.J. Cho, H. Morkoc, A comprehensive review of ZnO materials and devices, Journal of Applied Physics 98 (2005) 41301.
[21] Y.J. Kwon, K.H. Kim, C.S. Lim, K.B. Shim, Characterization of ZnO nanopowders synthesized by the polymerized complex method via an organochemical route, Journal of Ceramic Processing Research 3 (2002) 146–149.
[22] J. Matos, E.G. Lopez, L. Palmisano, A. Garcia, G. Marci, Influence of activated carbon in TiO_2 and ZnO mediated photo-assisted degradation of 2-propanol in gas–solid regime, Applied Catalysis B: Environmental 99 (2010) 170–180.
[23] O. Mekasuwandumrong, P. Pawinrat, P. Praserthdam, J. Panpranot, Effects of synthesis conditions and annealing post-treatment on the photocatalytic activities of ZnO nanoparticles in the degradation of methylene blue dye, Chemical Engineering Journal 164 (2010) 77–84.
[24] S.S. Alias, A.B. Ismail, A.A. Mohamad, Effect of pH on ZnO nanoparticle properties synthesized by sol–gel centrifugation, Journal of Alloys and Compounds 499 (2010) 231–237.
[25] S. Suwanboon, P. Amornpitoksuk, N. Muens, Dependence of photocatalytic activity on structural and optical properties of nanocrystalline ZnO powders, Ceramics International 37 (2011) 2247–2253.
[26] Y. Wu, J. Zhang, L. Xiao, F. Chen, Properties of carbon and iron modified TiO_2 photocatalyst synthesized at low temperature and photodegradation of acid orange 7 under visible light, Applied Surface Science 256 (2010) 4260–4268.
[27] P. Sagar, P.K. Shishodia, R.M. Mehra, H. Okada, A. Wakahara, A. Yoshida, Photoluminescence and absorption in sol–gel-derived ZnO films, Journal of Luminescence 126 (2007) 800–806.
[28] S. Fujihara, Y. Ogawa, A. Kasai, Tunable visible photoluminescence from ZnO thin films through Mg-doping and annealing, Chemistry of Materials 16 (2004) 2965–2968.
[29] J.Z. Kong, A.D. Li, H.F. Zhai, Y.P. Gong, H. Li, D. Wu, Preparation, characterization of the Ta-doped ZnO nanoparticles and their photocatalytic activity under visible-light illumination, Journal of Solid State Chemistry 182 (2009) 2061–2067.
[30] S. Maensiria, P. Laokula, V. Promarakb, Synthesis and optical properties of nanocrystalline ZnO powders by a simple method using zinc acetate dihydrate and polyvinyl pyrrolidone, Journal of Crystal Growth 289 (2006) 102–106.
[31] S. Suwanboon, Structural and optical properties of nanocrystalline ZnO powder from sol–gel method, Science Asia 34 (2008) 031–034.
[32] M. Risti, S. Musi, M. Ivanda, S. Popovi, Sol–gel synthesis and characterization of nanocrystalline ZnO powders, Journal of Alloys and Compounds 397 (2005) L1–L4.
[33] Y.Z. Li, D.S. Hwang, N.H. Lee, S.J. Kim, Synthesis and characterization of carbon-doped titania as an artificial solar light sensitive photocatalyst, Chemical Physics Letters 404 (2005) 25–29.
[34] H. Wang, C. Xie, W. Zhang, S. Cai, Z. Yang, Y. Gui, Comparison of dye degradation efficiency using ZnO powders with various size scales, Journal of Hazardous Materials 141 (2007) 645–652.
[35] Y.V. Kolenko, B.R. Churagulov, M. Kunst, L. Mazerolles, C. Colbeau-Justin, Photocatalytic properties of titania powders prepared by hydrothermal method, Applied Catalysis B: Environmental 54 (2004) 51–58.
[36] Z.L. Xu, J. Shang, C.M. Liu, C. Kang, H.C. Guo, Y.G. Du, The preparation and characterization of TiO_2 ultrafine particles, Materials Science and Engineering B 63 (1999) 211.